An efficient and thermally stable interconnecting layer for tandem organic solar cells

Feng Yang [a], Dong-Won Kang [b], Yong-Sang Kim [a,*]

[a] School of Electronic and Electrical Engineering, Sungkyunkwan University, Suwon, Gyeonggi 16419, Republic of Korea
[b] Department of Solar & Energy Engineering, Cheongju University, Cheongju, Chungbuk 28503, Republic of Korea

ARTICLE INFO

ABSTRACT

We report a novel interconnecting layer (ICL) consisting of MoO_3/Au/Al/ZnO for efficient operation of inverted homo-tandem organic solar cells employing poly(3-hexylthiophene) (P3HT) and (6,6)-phenyl C61-butyric acid methyl ester (PCBM). It was found that the ultrathin metal bilayer of Au/Al, a few nanometers, can align the energy levels and play a significant role in the charge extraction and recombination within the ICL. And the ICL showed an electrically ohmic-contact, high transmittance and very planar morphology for tandem application. The performance of air-fabricated homo-tandem organic solar cells with this new ICL delivered an average power conversion efficiency (PCE) of 3.0%, which is very close to the PCE of 3.3% from the state-of-the-art P3HT:PCBM based homo-tandem organic solar cells. Meanwhile, thermal stability tests at an elevated temperature of 150 °C for 12 h showed stable ICL with successful operation.

1. Introduction

The photovoltaic technology is growing up to its potential as a clean and renewable energy resource. Efficient organic solar cells with the advantages of low cost, easy fabrication process, stability, and flexibility, can be the great prospects of commercial applications for organic photovoltaics (OPVs) (Ameri et al., 2013). OPVs have been widely developed with the power conversion efficiency (PCE) of more than 10% by enormous research in last five years (You et al., 2013c, 2013a; Ouyang et al., 2015). Tandem concept attracts considerable research interest to overcome the energy losses in single cell OPV devices, such as narrow absorption spectra and thermalization loss (Sista et al., 2011). It is suggested that a maximum PCE of 21% is theoretically achievable for organic tandem solar cells by combining a front cell with a bandgap energy (E_g) of ≈ 1.6 eV and a rear cell with a E_g of ≈ 1.2 eV (Li et al., 2014). With the rapid development of novel materials and engineering techniques, the PCE of tandem OPVs recently has reached about 12% (Yusoff et al., 2015; Zhou et al., 2015; Chen et al., 2014a). There is still a room for the design of the tandem cells, because of the huge difference between the theoretical maximum PCE and the recently published works. Therefore, the tandem OPV devices

should provide a promising route to realize high performance organic solar cells.

Tandem OPVs research recently has been developed on two aspects: the synthesis of new donor (Dou et al., 2012) or acceptor (Li et al., 2016) materials for more efficient light absorption, and various designs of interconnection layer (ICL) with better charge extraction and recombination (Qing et al., 2014). The design of new materials has improved a lot in single junction organic solar cells (Ameri et al., 2013; Yip and Jen, 2012; You et al., 2013b). An efficient ICL is an important issue of tandem organic solar cells. In a typical tandem device, the two single sub-cells are stacked and connected by an ICL. The ICL generally consisted of a p-type hole transporting layer (HTL) and an n-type electron transporting layer (ETL), which function as the charge extraction and recombination layers (Zhou et al., 2015). The charge recombination depends on the alignment of Fermi levels of the HTL and ETL. There are some principles for the design of ICL. (1) ICL must have a high optical transmittance to minimize optical losses; (2) between the ETL and HTL, a quasi-ohmic-contact should be made to allow for electron-hole charge extraction and recombination; (3) the ICL should be robust enough to protect the underlying active layer from dissolution by the processing solvents for the top cell; and (4) The ICL should be environmentally stable to enhance the stability and lifetime of the tandem device (Ameri et al., 2013).

Many ICLs of tandem organic solar cells are reported. The typical ETLs in tandem OPV devices include transparent transition

* Corresponding author.
  E-mail address: yongsang@skku.edu (Y.-S. Kim).

metal oxides, such as ZnO (Chen et al., 2013; Kouijzer et al., 2012), TiO$_2$ (Yang et al., 2011; Kong et al., 2012) and polymer dipole layers (Yusoff et al., 2014; Zhou et al., 2012; Shim et al., 2012; Lu et al., 2015), such as PFN, CPE, PEIE. For HTL, metal oxides such as V$_2$O$_5$ (Chou et al., 2011), MoO$_3$, (Fan et al., 2013; Liu et al., 2014), and conductive polymers, such as PEDOT:PSS (Chang et al., 2012), are widely adopted in tandem organic solar cells. Also, some groups reported combined evaporation and solution approach ICLs such as MoO$_3$/Al/ZnO (Chou et al., 2011), and GO-Cs/Al/GO/MoO$_3$ (Chen et al., 2014b). Moreover, there are examples of evaporation based ICLs such Ca/Ag/MoO$_3$ (Fan et al., 2013), MoO$_3$/Ag/Al/Ca (Sun et al., 2010), and BCP/Ag/ReO$_3$ (Shim et al., 2014). However, efficient and thermally stable ICL is still a challenge for tandem organic solar cells. There are no papers studying on the thermal stability of ICL, but one paper (Kong et al., 2012) reported that they conducted the post-annealing with less than 150 °C for a few minutes. The post-annealing process is thought to induce an electrokinetic migration in which the mobile positive ions move toward/over the interface between TiOx and PEDOT:PSS. As a result, a dipole layer could formed in between the n-/p-type interlayers, originating from electrostatic acid-base interaction. It seems that the thermal stability of dipole layer in the ICL is sensitive or not much studied. To date, our research for first time reported the thermal stability of organic tandem solar cells.

In this work, we propose a new ICL of PEDOT:PSS/MoO$_3$/Au/Al/ZnO for tandem OPV devices, which is an efficient and thermally stable combination of different HTLs, metals, and ETL. For MoO$_3$ layer of the ICL, its performance is highly related the oxygen vacancies which is not much stable when exposed in the air. Energy level alignment can be achieved in MoO$_3$/Au through Fermi level pinning transition. The Au/Al bilayer effectively aligns the energy levels in the ICL. With metal–metal contact, the fermi levels of Au and Al were aligned without any energy barrier and were benefit for thermal resistance in this complex ICL structure of PEDOT:PSS/MoO$_3$/Au/Al/ZnO. Here, an ultrathin metal bilayer of Au/Al was suggested as a function of the charge recombination by aligning the energy levels and maintained a high transmittance. The inverted tandem organic solar cells based on poly(3-hexylthiophene) (P3HT) and (6,6)-phenyl C61-butyric acid methyl ester (PCBM) were fabricated by sandwiching the suggested ICL. It should be noted that the tandem cells were prepared without glovebox using inert gases since the glovebox-based process is expensive and laborious compared to the process under air-ambient (Sun et al., 2011). The performance of the air-fabricated homo-tandem organic solar cells an average PCE of 3.0%, which is very close to the PCE of 3.3% from the state-of-the-art P3HT:PCBM based homo-tandem organic solar cells (Lu et al., 2015). And the test of thermal stability at 150 °C for 12 h showed stable ICL with successful operation.

2. Experimental section

2.1. Materials

The indium tin oxide (ITO) coated glass was supplied by Fine Chemicals (South Korea) (15 Ω/square sheet resistance). Zinc acetate dihydrate (99.999%), monoethanolamine (MEA, ACS reagent, 99.0%), and 2-methoxyethanol (2-ME, anhydrous, 99.8%) were from Sigma Aldrich. Poly(3-hexylthiophene) (P3HT) was purchased from Rieke Metals and [6,6]-Phenyl C61 butyric acid methyl ester (PCBM) from Nano-C. Chlorobenzene, anhydrous, 99.9% was from Sigma Aldrich. PEDOT:PSS (Clevious PVP AI 4083) was supplied by Heroeus Deutschland GmbH & Co. KG (Germany). Triton X-100, extra pure, was supplied by Do Chemical Co., Ltd. Hexamethyldisilazane (HMDS) was purchased from AZ Electronic Materials (South Korea). Gold (Au) was from Vacuum Thin Film Materials Co. (South Korea) and Aluminum (Al), silver (Ag), MoO$_3$ (99.999%) from Alfa Aesar.

2.2. Single cell fabrication

The patterned ITO substrates were ultra-sonicated for 10 min in deionized water followed by acetone and then isopropyl alcohol. A 40 nm ZnO film, spin-coated from a ZnO precursor solution, was obtained on the ITO substrate (Yang et al., 2015). A 1:0.7 w/w blend of P3HT and PCBM, with the concentration of 10 mg/ml for P3HT, was dissolved in chlorobenzene by ultra-sonication for 4 h, filtered through a 0.45 μm PVDF filter, and spin-coated on the ZnO-coated ITO substrates. The formed active layer of P3HT:PCBM was ~60 nm in thickness. PEDOT:PSS solution was modified with 0.5% v/v of Triton X-100 nonionic surfactant (Yang et al., 2016). HMDS was first spin-coated on the active layer, followed by the PEDOT:PSS deposition. The modified PEDOT:PSS was spin-coated on the active layer and annealed in an oven at 160 °C for 10 min. A PEDOT:PSS film of 30–40 nm was obtained on the active layer. The devices were prepared for measurement after the thermal deposition of ~100 nm thick Ag film through a shadow mask. All fabrication processes were carried out in the ambient air except vacuum thermal deposition process of silver. The active area of each device was defined by the overlap between the patterned ITO and Ag electrodes, 0.09 cm^2.

2.3. Tandem device fabrication

The front cells were made according to the single cells procedure before deposition of Ag, and then the samples were transferred into the evaporation chamber. 10 nm MoO$_3$, 3 nm Au and 2 nm Al (without breaking the vacuum) were subsequently thermally evaporated on top of the front cell at 6×10^{-6} Torr. An amorphous ZnO layer was deposited with a precursor solution consisting of 0.3 M zinc acetate and 0.3 M monoethanolamine in 2-methoxyethanol at a spin speed of 4000 rpm for 40 s. The film was annealed at 150 °C for 10 min in ambient air. The active layer and PEDOT layer of top sub-cells were made according to the single cells procedure. Finally, 100 nm of silver as the anode was thermally evaporated through a shadow mask. The device area, as defined by the overlap between the patterned ITO and Ag electrodes, was 0.09 cm^2. 1:1:0.1 (or 1:1:0.2) w/w blends of P3HT:PCBM:pentacene for active layer of modified the sub-cells were dissolved in chlorobenzene by ultra-sonication of 4 h, filtered with a 0.45 μm PVDF filter, and spin-coated on the ZnO film.

2.4. Device characterization

The current density - voltage (*J-V*) characterization of devices was measured with J-V curve tracer (Eko MP-160) and a solar simulator (Yss-E40, Yamashita Denso) under AM 1.5G irradiation with the intensity of 100 mW/cm^2, calibrated by Newport certified standard silicon cell. The transmittance spectroscopy measurements were made over a wavelength range of 200–900 nm using a Shimadzu UV-1601 UV–Vis spectrophotometer (the transmittance of 0.7 mm thick of glass substrate was measured as the base). Optical microscopy images were obtained using an Olympus BX41 Microscope Digital Camera. Atomic force microscopy (AFM) images were obtained with an advanced scanning probe microscopes (PSIA Corp). The thicknesses of all films were characterized by the AFM system. The thermal stability measurements of tandem solar cells were taken at an elevated temperature of 150 °C on a hotplate in ambient air.

3. Results and discussion

Fig. 1(a) and (b) shows the energy level diagram and device structure of the inverted tandem organic solar cells with an ICL of PEDOT:PSS/MoO₃/Au/Al/ZnO. Both the sub-cells in the tandem device were based on P3HT and PCBM blends active layers. Even though sub-cells consisting of the different bandgap can utilize more solar spectrum, however, the development and realization of the ICL for OPVs is our main interest in this study. Hence, the same active layers were constructed for the both sub-cells. There are four advantages of the ICL for tandem OPV devices. Firstly, the active layer of P3HT:PCBM was covered with PEDOT:PSS before further annealing process, which keeps the active layer out of air and saves its life-time. Secondly, the super-thin bilayer of gold (Au) and aluminum (Al) serves to align the Fermi levels in the ICL and to form the quasi-ohmic-contact. Thirdly, the ZnO film is very dense and robust to further coating process of the second

sub-cell. Lastly, a 10 nm MoO₃ film, between the PEDOT:PSS and ZnO, can protect the underlying sub-cell from the ZnO precursor solution. In order to design an efficient ICL for the inverted tandem device, which is fabricated in the ambient air, the air-sensitive P3HT:PCBM film was covered with a buffer layer. Fig. 2 (a) and (b) shows the performance of sub-cells decreased by one about a half when the active layer of P3HT:PCBM was aged for 20 h in the air without the buffer layer of PEDOT:PSS. The short current density (J_{SC}) and PCE showed quite a decrease in a few hours. To save the sub-cell, the P3HT:PCBM film was covered with PEDOT:PSS before thermal treatment. Fig. 2(b) shows that the PCE of P3HT:PCBM film covered with PEDOT:PSS was greatly more stable than that without PEDOT:PSS during the aging process in the air. The metal layers of gold and aluminum serve as the charge recombination layer, which is very important for the charge recombination of electrons extracted from top sub-cell and holes from bottom sub-cell. The reason we used a bilayer of Au/Al, is
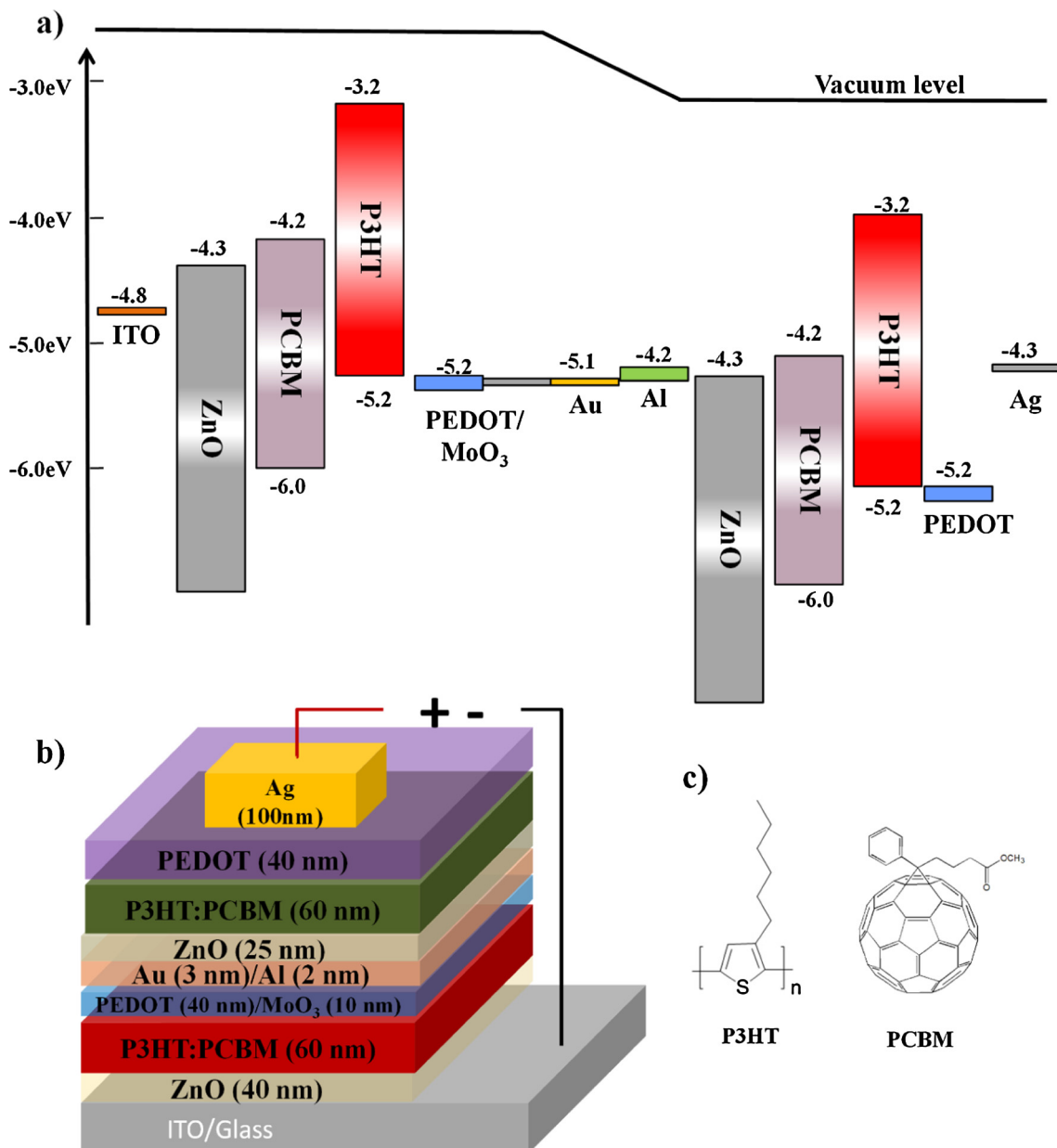
Fig. 1. Energy level diagram and device structure of tandem organic solar cells. (a) Energy level diagram of individual layers used in tandem OPV devices. (b) Tandem device structure. (c) Molecular structures of active layer, P3HT and PCBM.
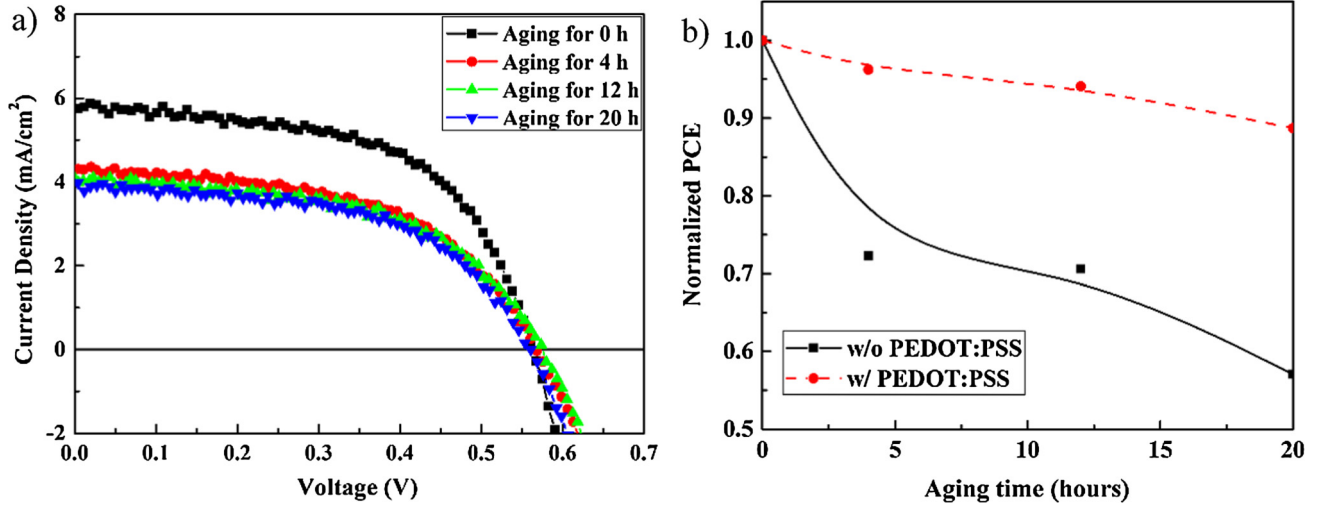
Fig. 2. (a) Current density–voltage (J-V) characteristics of single sub-cell with various air aging time on the active layer of P3HT:PCBM; (b) normalized PCE of single sub-cell with various air aging time on the active layer covered with (w/) or without (w/o) PEDOT:PSS.

to effectively shift the vacuum levels (as shown in Fig. 1a), and to make a quasi-ohmic-contact in the ICL. The charge recombination layer is very thin to be highly transparent. The thickness of Au film is only 3 nm and the Al is 2 nm. The ETL in the ICL is ZnO, which is a very dense film and robust to chlorobenzene. The Al film also acts as a wetting layer for the ZnO deposition (Chou et al., 2011). We performed the thermal treatment for three times at more than 150 °C in the fabrication process of tandem devices. The thermal stability of active layers and ICL is very important for the performance of the tandem organic solar cells.

The good electric property of the ICL is very necessary to the tandem solar cells. It was studied in depth by measuring dark J-V characteristics of various ICLs sandwiched between ITO and Ag electrodes, as shown in Fig. 3. Without the charge recombination layer of Au/Al, the energy barrier of ICL-1 (PEDOT:PSS/ZnO), were large as expected. ICL-1 is a typical PN junction as shown in the J-V curve. The series resistance of ICL-1 is also large, 1027.6 Ohm cm^2, as shown in Table 1. The mismatched energy levels in the interconnecting layer result in a large series resis-

Table 1
The resistance (R) of ICL layers from the dark J-V curves at 1.0 V. Various interconnecting layer (ICL) sandwiched between ITO and Ag; ICL-1 of PEDOT:PSS/ZnO, ICL-2 of PEDOT:PSS/Au/Al/ZnO, ICL-3 of PEDOT:PSS/MoO$_3$/Au/Al/ZnO.

ICL devices	R at 1.0 V [Ohm cm^2]
ICL-1	1027.6
ICL-2	4.7
ICL-3	3.9
ITO/ZnO/Ag	3.0

tance. But the ICL-2 (PEDOT:PSS/Au/Al/ZnO) with the charge recombination layer of Au/Al, could shift of energy levels in ICL. When the thin Au and Al films contacted with each other, their Fermi levels (E_F) in the ICL-2 are aligned naturally, which will lead to a quasi-ohmic-contact in the ICL. The dark J-V curves were linear as shown in Fig. 3, indicating the ohmic-contact. The ICL-3 (PEDOT:PSS/MoO$_3$/Au/Al/ZnO) shows similar ohmic-contact as ICL-2. The series resistance of ICL-3, 3.9 Ohm cm^2, is smaller than that of ICL-2, 4.7 Ohm cm^2, as shown in Table 1. And a similar structure of ITO/ZnO/Ag, those energy levels are well matched, was as reference structure with a series resistance of 3.0 Ohm cm^2. The resistances of ICL-2 and ICL-3 with the charge recombination layer of Au/Al, 4.7 and 3.9 Ohm cm^2, respectively, are almost the same order as the reference device, 3.0 Ohm cm^2, as shown in Table 1. But the resistance of ICL without the charge recombination layer of Au/Al, is almost three orders higher than that of ICL with the Au/Al layers. The ICL-3 has the lowest resistance of all ICLs because of the insertion of MoO$_3$ between PEDOT:PSS and ZnO layers which protects PEDOT:PSS layer from possible deterioration by solvents in ZnO precursor solution. It is suggested that the ICL-3 structure is more suitable for the ICL of the tandem solar cells.

Fig. 4 primarily presents the optical transmittance spectra of the sub-layers of ICL. Since the thickness of metal layers of Au or Al are in 2–3 nm, the transmittance of any one of these layers were higher than 97% in the whole visible light region. The ZnO film has a slightly higher transmittance, more than 98%, at wavelengths longer than 400 nm, but decreases to 85% at the wavelengths of 320 nm, related with the energy bandgap of the ZnO film. Two different research groups reported the similar transmittance of ZnO film at 400 nm, ca. 98% (Lin et al., 2014) and 95% (Oh et al.,
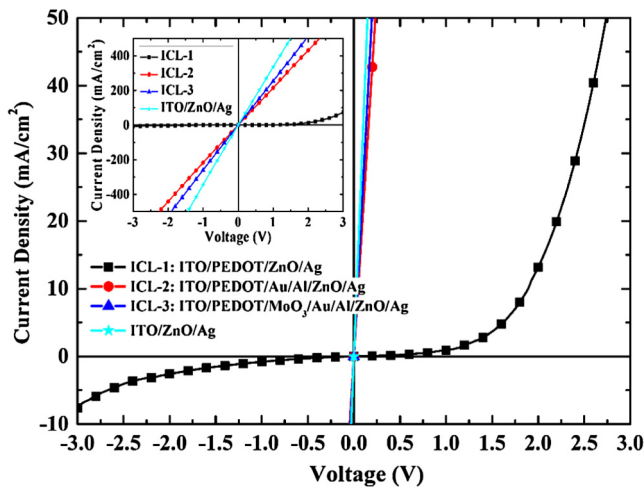
Fig. 3. The dark J-V characteristics of various interconnecting layer (ICL) sandwiched between ITO and Ag, such as ICL-1 of PEDOT:PSS/ZnO, ICL-2 of PEDOT:PSS/Au/Al/ZnO, ICL-3 of PEDOT:PSS/MoO$_3$/Au/Al/ZnO, and reference device of ITO/ZnO/Ag. The inserted figure shows Dark J-V characteristics of the various ICL with large scale of 1000 mA/cm^2.
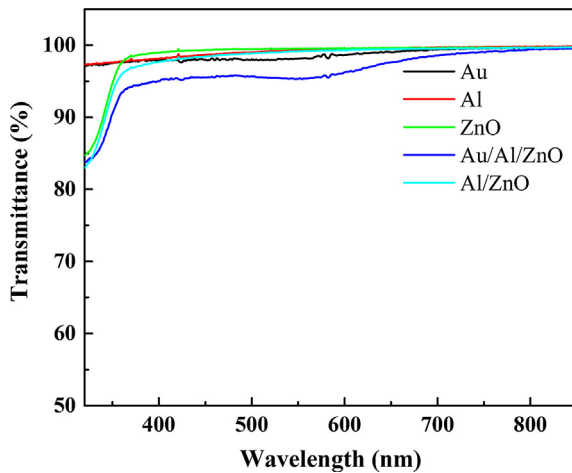
Fig. 4. UV–visible transmittance spectra of thin films of Au, Al, ZnO, Au/Al/ZnO, and Al/ZnO.

Fig. 5. Optical microscopy images of the surfaces of interconnecting layer on (a) 60 nm P3HT:PCBM 1:0.7, and (b) 60 nm P3HT:PCBM 1:0.8 organic sub-cells. Scale bar = 100 μm.

2011), respectively. The transmittance of combined layer of Au/Al/ZnO is more than 95% at the wavelengths longer than 400 nm. Thus, the incident light passes through the bottom sub-cell and will easily go through the ICL with little absorption or reflection. After that the light will be absorbed in the top sub-cell and contribute to photovoltaic current. As all we know that PEDOT:PSS and MoO_3 have high optical property and are in popular use in organic solar cells. Then, the ICL of PEDOT:PSS/MoO_3/Au/Al/ZnO is with high optical transmittance and suitable for tandem organic solar cells.

The thermally stable active layer of P3HT:PCBM was obtained by the suppressing the crystallization of PCBM. During thermal annealing process, the PCBM molecules start to slowly aggregate and form micrometer-sized crystals (Kesters et al., 2014). The PCE of the OPV devices could decrease a lot because of the crystallite over-growth of PCBM (Yang et al., 2015). However, the thermal stability of P3HT:PCBM could be improved by suppressing PCBM crystallites with the ZnO substrates (Li et al., 2015). The crystallization of PCBM could be further suppressed with the deposition of PEDOT:PSS before thermal treatment. The surface details of P3HT:PCBM with various ratios, 1:0.6, 1:0.7, 1:0.8, and 1:0.9 were shown in supporting information Fig. S1. During thermal annealing process, the PCBM molecules start to slowly aggregate and form micrometer-sized crystals as shown in Fig. S1(c) and (d). The thermal stability of P3HT:PCBM surface could be improved when reducing PCBM in the P3HT:PCBM layer by 1:0.6, 1:0.7, while the PCBM crystals showed up on the surface of P3HT:PCBM layer of 1:0.8 and 1:0.9. The microscope morphology of ICL deposited on the bottom sub-cells was shown in Fig. 5. The surface property of ICLs on different bottom sub-cells are remarkably different. The PCBM crystals in the sub-cell, induce many defects in the ICL, as shown in Fig. 5(b). The round defects are also found in the 60 nm P3HT:PCBM 1:0.8 sub-cell (Fig. 5b). However, Fig. 5 (a) shows that the clear surface of ICL was obtained on the clear surface of 60 nm P3HT:PCBM 1:0.7 sub-cell. Finally an uniform ICL was realized with a thin P3HT:PCBM 1:0.7 sub-cell of 60 nm.

The topography and surface roughness of the ICL were investigated by atomic force microscopy in Fig. 6. Fig. 6(a) shows PEDOT:PSS surface of the bottom sub-cell with a root mean square (RMS) of 0.97 nm. Fig. 6(b) shows that the sub-cell is fully covered with MoO_3 with an RMS of 0.32 nm, because its RMS value was very small, and the sub-cell with MoO_3 had a very flat surface. After depositing the metal bilayer of ICL, the surface of Au/Al bilayer became flatter as shown in Fig. 6(c), since its RMS was 0.26 nm.
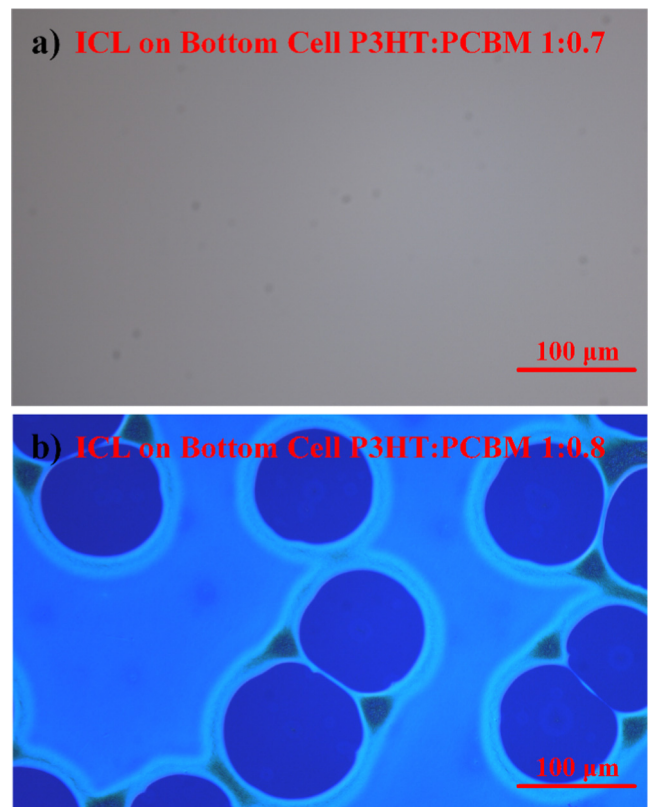
The ICL surface was very clean, without any PCBM particles. The ICL was completed with spin-coating ZnO film on the metal bilayer. After thermal treatment at 150 °C for 10 min, the ICL was uniform (as shown in Fig. 6d) since its surface RMS was 0.20 nm. The topography images show that the ICL of PEDOT:PSS/MoO_3/Au/Al/ZnO can provide favorable surface at the interfaces between the two sub-cells in the tandem device. Because the ZnO ETL needs a thermal treatment process, the organic bottom sub-cell should meet the thermal stability especially for the active layer.

Simple ICLs have been effectively used in many organic tandem devices, such as ZnO/ PEDOT:PSS (Chen et al., 2014a), TiOx/PEDOT:PSS (Kong et al., 2012), ethoxylated polyethylenimine (PEIE)/PEDOT:PSS (bin Mohd Yusoff et al., 2014), MoOx/Ag/PEIE (Shim et al., 2012), ZnO/ conjugated polyelectrolyte (CPE), (Zhou et al., 2015), MoOx/dipole/TiO2, (Lu et al., 2015). Typically, the electron-hole recombination center of these ICLs are from dipole layer formed between the n-type and p-type layer. And the gap states caused by oxygen vacancies in the transition metal oxide (Greiner et al., 2013) act as dopants which benefit the electron-hole pair recombination and conductivity of ICL. However, these dipole layers usually are sensitive to the thermal treatment at high temperature, because they are mainly from the weak organic chemical group or ions imgration. Even, the thin metal layer was introduced as charge recombination layer, such as MoO_3/Ag/Al/ZnO (Qing et al., 2014), MoO_3/Al/ZnO (Chou et al., 2011). The fill factor of tandem devices is mostly less than 0.6 since the Schottky barrier is not fully reduced in the ICL. Especially for MoO_3 layer, its performance is highly related the oxygen vacancies. Energy level alignment can be achieved in MoO_3/Au through Fermi level pinning transition. Fig. 7 shows the schematic energy level diagrams of ICL of (a) MoO_3/Au/Al/ZnO, (b) MoO_3/Au/ZnO, and (c) MoO3/

a) Bottom sub-cell

b) Bottom sub-cell/MoO$_3$

c) Bottom sub-cell/MoO$_3$/Au/Al

d) Bottom sub-cell/MoO$_3$/Au/Al/ZnO
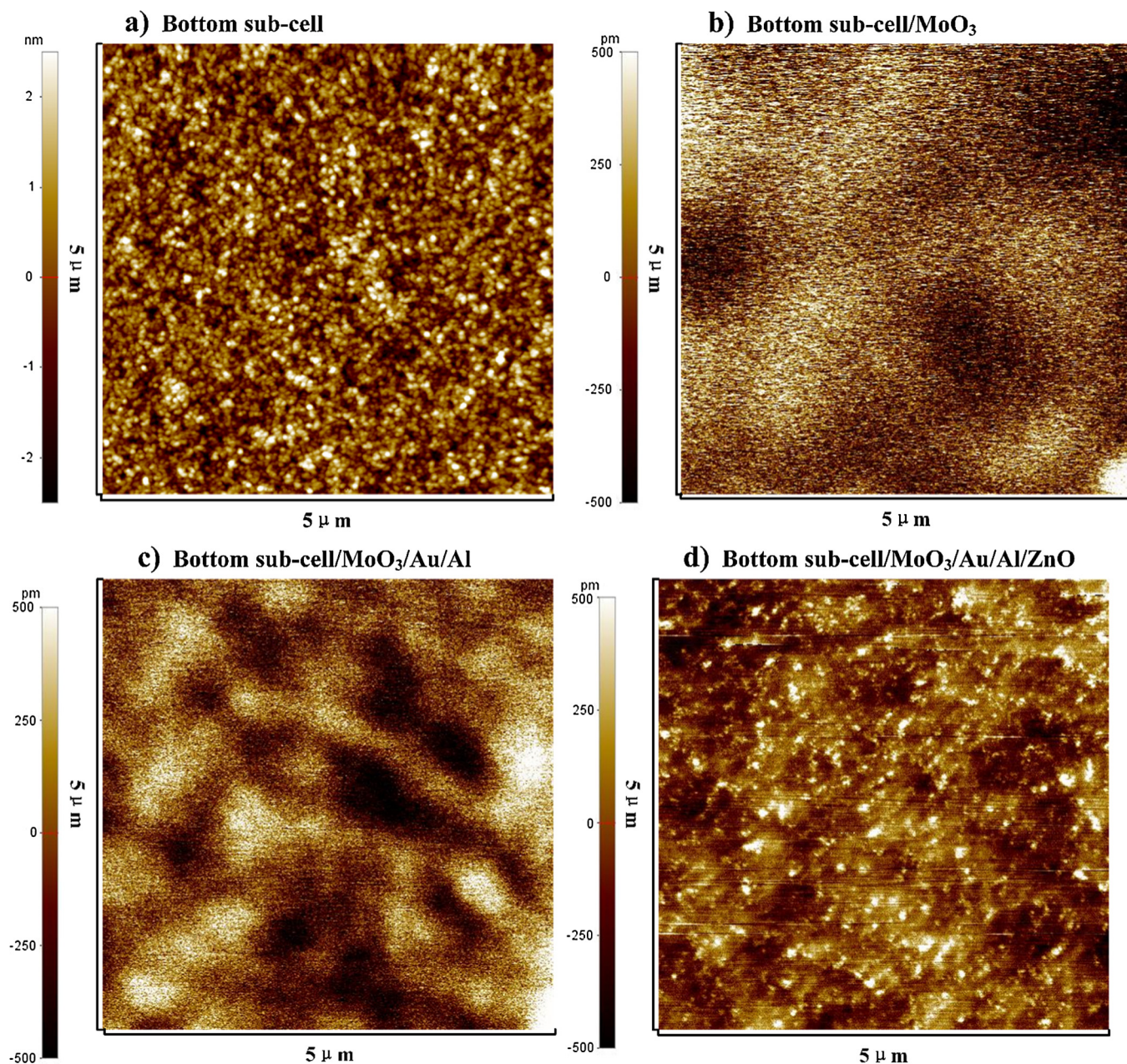
Fig. 6. Atomic force microscopy topography images of individual sub-layer of interconnecting layers on bottom sub-cell (ITO/ZnO/P3HT:PCBM/PEDOT:PSS), (a) bottom sub-cell, RMS = 0.97 nm; (b) bottom sub-cell/MoO$_3$, RMS = 0.32 nm; (c) bottom sub-cell/MoO$_3$/Au/Al, RMS = 0.26 nm; and (d) bottom sub-cell/MoO$_3$/Au/Al/ZnO, RMS = 0.20 nm. The size of all images is 5 μm × 5 μm.

Al/ZnO. It is very easy to figure out that the Au/Al bilayer effectively aligned the energy levels in the ICL. Because of metal–metal contact, the fermi levels of Au and Al were aligned without any energy barrier. All in all, it is reasonable to apply a metallic bilayer of Au/Al for an air stable and thermally stable ICL.

The current density–voltage (*J-V*) characteristics of single and tandem devices are shown in Fig. 7(d). And Table 2 shows the photovoltaic performances of the single sub-cells and tandem devices. The tandem device A with PEDOT:PSS/ZnO ICL, without the metal bilayer (Au/Al), had poor open-circuit voltage (*Voc*) and fill factor (FF). Because of no wetting effect of super-thin Al film, the dense ZnO film is very hard to be casted on the PEDOT:PSS/MoO$_3$ surface. When we coated the top sub-cell, the chlorobenzene solvent would penetrate the ICL layer and the two sub-cells would be joined into one junction. It would be seriously detrimental to the *Voc* and FF.

In case of the tandem device B with PEDOT:PSS/MoO$_3$/Al/ZnO ICL, the *Voc* improved from 0.48 to 1.09 V, whereas the FF was still much smaller than single sub-cell because there is not successful energy level alignment and efficient charge recombination in the ICL (Fig. 7c). However, the tandem device C with PEDOT:PSS/MoO$_3$/Au/Al/ZnO ICL showed a very good PCE of 3.04%. As shown in Fig. 7(d), the V_{OC} of homo-tandem devices is almost twice as much as that of the single devices. And the FFs of the single sub-cells and tandem devices are similar. The small J_{SC} of tandem device comes from the less light reflection back to the bottom sub-cell, because the light goes through the very thin bottom sub-cell and is secondly absorbed in top sub-cell when light is reflected back by the silver electrode of top sub-cell. Compared to other three ICLs, there was significant improvement in performance of tandem device C. The tandem device C with an efficient
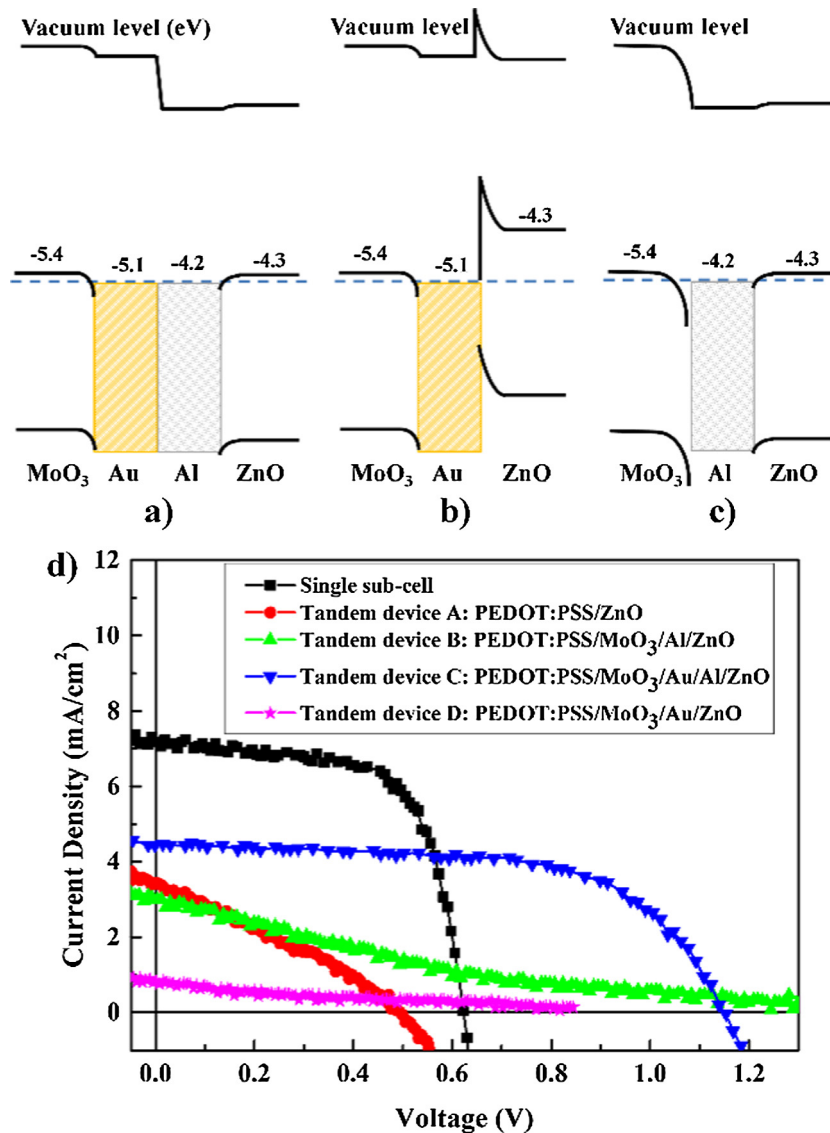
Fig. 7. Schematic energy level diagrams of ICL of (a) MoO_3/Au/Al/ZnO, (b) MoO_3/Au/ZnO, and (c) MoO_3/Al/ZnO. (d) Current density–voltage characteristics of single cell and tandem OPV devices. Tandem solar cells with various interconnecting layers, tandem device A of PEDOT:PSS/ZnO, tandem device B of PEDOT:PSS/MoO_3/Al/ZnO, tandem device C of PEDOT:PSS/MoO_3/Au/Al/ZnO, and tandem device D of PEDOT:PSS/MoO_3/Au/ZnO.

Table 2
Photovoltaic parameters of single sub-cell and various tandem OPV devices. The standard deviation in brackets and the average performance were from 6 devices. Tandem device A of PEDOT:PSS/ZnO, tandem device B of PEDOT:PSS/MoO_3/Al/ZnO, tandem device C of PEDOT:PSS/MoO_3/Au/Al/ZnO, and tandem device D of PEDOT:PSS/MoO_3/Au/ZnO.

Devices	J_{SC} [mA/cm^2]	V_{OC} [V]	FF	PCE [%]
Single Sub-cell	7.15 (±0.26)	0.62 (±0.00)	0.63 (±0.02)	2.83 (±0.11)
Tandem Device A	2.86 (±0.28)	0.48 (±0.02)	0.30 (±0.00)	0.41 (±0.05)
Tandem Device B	2.96 (±0.14)	1.09 (±0.03)	0.21 (±0.00)	0.66 (±0.03)
Tandem Device C	4.35 (±0.16)	1.11 (±0.03)	0.63 (±0.02)	3.04 (±0.08)
Tandem Device D	0.75 (±0.04)	0.85 (±0.09)	0.24 (±0.02)	0.15 (±0.02)

ICL showed the highest average V_{OC} of 1.11 V. The average J_{SC} and FF were around 4.35 mA/cm^2 and 0.63, respectively. With the metal bilayer of Au/Al between the HTL and ETL, the ICL works effectively as electrically quasi-ohmic contact (Fig. 7a). The ohmic-contact interface of Au/Al can improve the charge extraction and charge recombination at the ICL. In tandem device D with PEDOT:PSS/MoO_3/Au/ZnO ICL, it could meet a huge energy barrier inside the ICL (Fig. 7b). The contact of Au/ZnO cannot form a quasi-ohmic contact but a Schottky contact. Hence, the J_{SC} of tandem device D was very low. Thus, these experimental results demonstrate that the suggested metal bilayer of Au/Al aligns the energy levels in the ICL and plays a very important role in electric property.

Fig. 8 shows the thermal stability measurement of non-encapsulated tandem organic solar cells. It should be noted that thermal stability is a key issue for commercializing organic tandem solar cells, such as thermal encapsulation processing of ethylene vinyl acetate or high-temperature atomic layer deposition. The
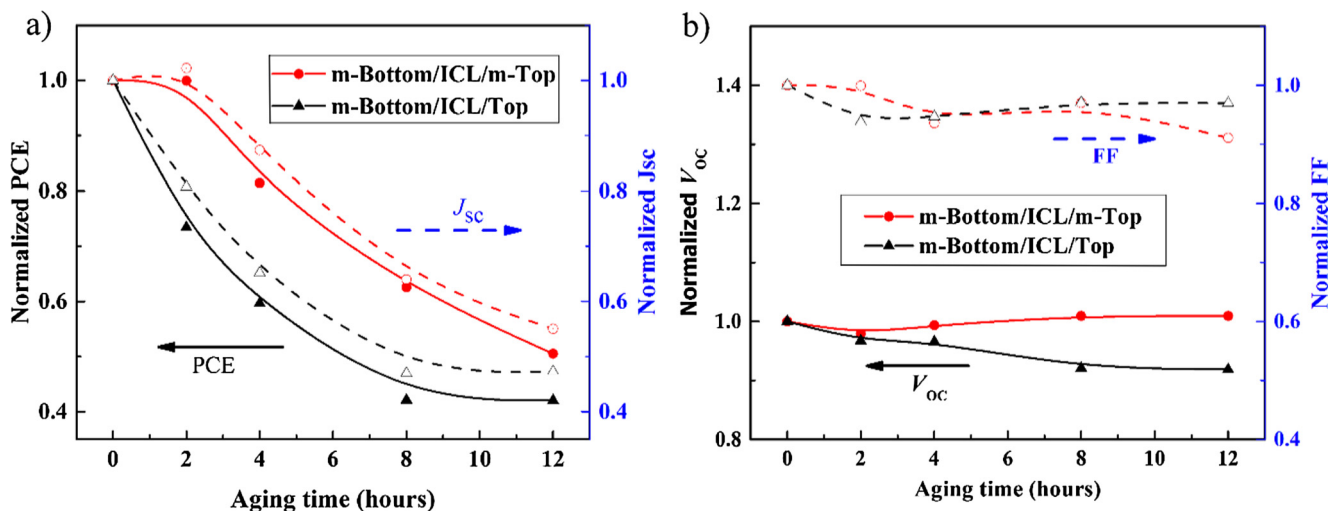
Fig. 8. The thermal stability of tandem organic solar cells with pentacene modified bottom sub-cell (m-Bottom) or top sub-cell (m-Top) as a function of time when annealed at 150 °C in ambient air. (a) Normalized PCE and J_{SC}, (b) Normalized V_{OC} and FF of the different types of tandem OPV devices annealed at 150 °C over time.

PCE of tandem OPVs was decreased when aged at 150 °C for several hours. Since a tandem solar cells consist of two organic sub-cells and an ICL, the overall thermal stability of the tandem devices depends on thermal stability of both sub-cells and ICL. The two organic sub-cells in tandem devices typically are sensitive to the thermal aging process (Fig. S1a) and their thermal stability can be improved by the modified organic sub-cells with pentacene (Yang et al., 2015). In order to keep thermally stable morphology of ICL during the aging time, we modified the thermal stability of sub-cells with pentacene. With these thermally stable sub-cells, there is a way to characterize the thermal stability of the ICL and the whole organic tandem solar cells. We implied that the ICL is the main reason for the high thermal stability of organic tandem solar cells because the sub-cells could be replaced with some thermal stable active layers with other treatment (Grant et al., 2017; Li et al., 2017; Salim et al., 2016).

Two types of tandem OPVs, m-Bottom/ICL/m-Top and m-Bottom/ICL/Top, were designed for characterizing the thermal stability of ICL. The modified sub-cells with pentacene (P3HT:PCBM: Pentacene of 1:1:0.1) were used as bottom sub-cell (m-Bottom) in both the two types of tandem devices and the modified top sub-cell (m-Top) was only used for m-Bottom/ICL/m-Top tandem device. Fig. 8(a) shows that the PCE and J_{SC} of the tandem OPVs of m-Bottom/ICL/m-Top were thermally stable within the first two hours of the aging process. But the PCE and J_{SC} of tandem OPVs of m-Bottom/ICL/Top, with non-modified top sub-cell, decreased a lot at the beginning of the aging process. The decrease of J_{SC} came from the non-modified active layer during the thermal aging process similar as in Fig. S2 (a) (supporting information), while the single cells modified with pentacene were thermally stable. The thermal aging process leads to the formation of large size PCBM aggregates in the non-modified active layer (Yang et al., 2015), which reduces the electron transport pathways within the active layer and thus increases the charge recombination losses (Wang et al., 2015). The aggregates of PCBM and P3HT reduce large interfacial area between P3HT and PCBM and also hamper charge dissociation, as confirmed by a decrease in J_{SC} (Bertho et al., 2013). These led to dramatic decrease in the J_{SC}, Voc, and PCE of the non-modified organic single cells as shown in Fig. S2. The PCE and J_{SC} of the tandem OPVs with modified top-cells were more stable than these without m-Top sub-cells (Fig. 8a). Thus, the main reduction of the J_{SC} of tandem OPVs came from these changes in the sub-cells. The thermal stability of ICL is related to J_{SC}, FF and V_{OC} of

the tandem OPVs. Even though the J_{SC} dropped due to deterioration of active layer of sub-cells, it is quite impressive that the FF and V_{OC} of tandem devices only reduced less than 10% against the thermal aging process for 12 h. The V_{OC} of tandem devices with non-modified top sub-cell gradually dropped less than 10%, which is similar as V_{OC} of non-modified single cells dropped in Fig. S2(b). The FFs of the two types of tandem device dropped less than 10% because of the FF losses of modified or non-modified sub-cells. These suggest that the thermal stability of the ICL in tandem OPVs works essential to electrically connect each sub-cell in this architecture. On the basis of these experimental examination, the novel ICL can be effectively applied for highly efficient, stable interconnection for the monolithic tandem OPVs.

4. Conclusions

In this study, efficient homo-tandem organic solar cells based on the P3HT:PCBM blends have been successfully fabricated in ambient air using a novel interconnecting layer of PEDOT:PSS/MoO$_3$/Au/Al/ZnO. The performance of tandem OPV device comes from the sub-cells with a 60 nm thick active layer of P3HT:PCBM, achieving an average power conversion efficiency (PCE) of 3.0% with J_{SC} = 4.35 mA/cm^2, open-circuit voltage (V_{OC}) = 1.11 V, and fill factor (FF) = 0.63. The tandem device with this novel ICL exhibits the similar FF values as those of single junction cells. It also demonstrates that the ICL does not add detrimental series resistance. The ultra-thin metal bilayer of Au/Al can align the energy levels and play a significant role in the charge extraction and recombination within the ICL. The optimized ICL was found to have pronounced electric, optical, and robust properties. The thermal stability of the ICL at 150 °C in tandem OPVs works essential to electrically connect each sub-cell in this architecture. All in all, the proposed efficient and thermally stable ICL demonstrates a promising chance for the air stable and highly efficient tandem organic solar cells and their commercial application.

Appendix A. Supplementary material

Supplementary data associated with this article can be found, in the online version, at http://dx.doi.org/10.1016/j.solener.2017.06.054.

References

Ameri, T., Li, N., Brabec, C.J., 2013. Highly efficient organic tandem solar cells: a follow up review. Energy Environ. Sci. 6 (8), 2390–2413.

Bertho, S., Campo, B., Piersimoni, F., Spoltore, D., D'Haen, J., Lutsen, L., Maes, W., Vanderzande, D., Manca, J., 2013. Improved thermal stability of bulk heterojunctions based on side-chain functionalized poly(3-alkylthiophene) copolymers and PCBM. Sol. Energy Mater. Sol. Cells 110, 69–76.

Bin Mohd Yusoff, A.R., Lee, S.J., Kim, H.P., Shneider, F.K., da Silva, W.J., Jang, J., 2014. 8.91% power conversion efficiency for polymer tandem solar cells. Adv. Funct. Mater. 24 (15), 2240–2247.

Chang, L., Holmes, M.A., Waller, M., Osterloh, F.E., Moule, A.J., 2012. Calcium niobate nanosheets as a novel electron transport material for solution-processed multi-junction polymer solar cells. J. Mater. Chem. 22 (38), 20443–20450.

Chen, C.-C., Chang, W.-H., Yoshimura, K., Ohya, K., You, J., Gao, J., Hong, Z., Yang, Y., 2014a. An efficient triple-junction polymer solar cell having a power conversion efficiency exceeding 11%. Adv. Mater. 26 (32), 5670–5677.

Chen, Y.-L., Kao, W.-S., Tsai, C.-E., Lai, Y.-Y., Cheng, Y.-J., Hsu, C.-S., 2013. A new ladder-type benzodi(cyclopentadithiophene)-based donor-acceptor polymer and a modified hole-collecting PEDOT:PSS layer to achieve tandem solar cells with an open-circuit voltage of 1.62 V. Chem. Commun. 49 (70), 7702–7704.

Chen, Y., Lin, W.-C., Liu, J., Dai, L., 2014b. Graphene oxide-based carbon interconnecting layer for polymer tandem solar cells. Nano Lett. 14 (3), 1467–1471.

Chou, C.-H., Kwan, W.L., Hong, Z., Chen, L.-M., Yang, Y., 2011. A metal-oxide interconnection layer for polymer tandem solar cells with an inverted architecture. Adv. Mater. 23 (10), 1282–1286.

Dou, L., You, J., Yang, J., Chen, C.-C., He, Y., Murase, S., Moriarty, T., Emery, K., Li, G., Yang, Y., 2012. Tandem polymer solar cells featuring a spectrally matched low-bandgap polymer. Nat. Photon. 6 (3), 180–185.

Fan, X., Guo, S., Fang, G., Zhan, C., Wang, H., Zhang, Z., Li, Y., 2013. An efficient PDPPTPT:PC61BM-based tandem polymer solar cells with a Ca/Ag/MoO₃ intermediate layer. Sol. Energy Mater. Sol. Cells 113, 135–139.

Grant, T.M., Gorisse, T., Dautel, O., Wantz, G., Lessard, B.H., 2017. Multifunctional ternary additive in bulk heterojunction OPV: increased device performance and stability. J. Mater. Chem. A 5 (4), 1581–1587.

Greiner, M.T., Chai, L., Helander, M.G., Tang, W.-M., Lu, Z.-H., 2013. Metal/metal-oxide interfaces: how metal contacts affect the work function and band structure of MoO₃. Adv. Funct. Mater. 23 (2), 215–226.

Kesters, J., Kudret, S., Bertho, S., Van den Brande, N., Defour, M., Van Mele, B., Penxten, H., Lutsen, L., Manca, J., Vanderzande, D., Maes, W., 2014. Enhanced intrinsic stability of the bulk heterojunction active layer blend of polymer solar cells by varying the polymer side chain pattern. Org. Electron. 15 (2), 549–562.

Kong, J., Lee, J., Kim, G., Kang, H., Choi, Y., Lee, K., 2012. Building mechanism for a high open-circuit voltage in an all-solution-processed tandem polymer solar cell. Phys. Chem. Chem. Phys. 14 (30), 10547–10555.

Kouijzer, S., Esiner, S., Frijters, C.H., Turbiez, M., Wienk, M.M., Janssen, R.A.J., 2012. Efficient inverted tandem polymer solar cells with a solution-processed recombination layer. Adv. Energy Mater. 2 (8), 945–949.

Li, J.L., Zhu, X.G., Yuan, T., Shen, J.L., Liu, J.K., Zhang, J., Tu, G.L., 2017. Donor acceptor interface stabilizer based on fullerene derivatives toward efficient and thermal stable organic photovoltaics. ACS Appl. Mater. Interfaces 9 (7), 6615–6623.

Li, N., Baran, D., Spyropoulos, G.D., Zhang, H., Berny, S., Turbiez, M., Ameri, T., Krebs, F.C., Brabec, C.J., 2014. Environmentally printing efficient organic tandem solar cells with high fill factors: a guideline towards 20% power conversion efficiency. Adv. Energy Mater. 4 (11), 1400084.

Li, S., Liu, W., Shi, M., Mai, J., Lau, T.-K., Wan, J., Lu, X., Li, C.-Z., Chen, H., 2016. A spirobifluorene and diketopyrrolopyrrole moieties based non-fullerene acceptor for efficient and thermally stable polymer solar cells with high open-circuit voltage. Energy Environ. Sci. 9 (2), 604–610.

Li, Z., Ho Chiu, K., Shahid Ashraf, R., Fearn, S., Dattani, R., Cheng Wong, H., Tan, C.-H., Wu, J., Cabral, J.T., Durrant, J.R., 2015. Toward improved lifetimes of organic solar cells under thermal stress: substrate-dependent morphological stability of PCDTBT:PCBM films and devices. Sci. Rep. 5, 15149.

Lin, Z., Chang, J., Jiang, C., Zhang, J., Wu, J., Zhu, C., 2014. Enhanced inverted organic solar cell performance by post-treatments of solution-processed ZnO buffer layers. RSC Adv. 4 (13), 6646–6651.

Liu, J., Shao, S., Fang, G., Wang, J., Meng, B., Xie, Z., Wang, L., 2014. High-efficiency inverted tandem polymer solar cells with step-Al-doped MoO₃ interconnection layer. Sol. Energy Mater. Sol. Cells 120, 744–750.

Lu, S., Guan, X., Li, X., Sha, W.E.I., Xie, F., Liu, H., Wang, J., Huang, F., Choy, W.C.H., 2015. A new interconnecting layer of metal oxide/dipole layer/metal oxide for efficient tandem organic solar cells. Adv. Energy Mater. 5 (17), 1500631.

Oh, H., Krantz, J., Litzov, I., Stubhan, T., Pinna, L., Brabec, C.J., 2011. Comparison of various sol-gel derived metal oxide layers for inverted organic solar cells. Sol. Energy Mater. Sol. Cells 95 (8), 2194–2199.

Ouyang, X., Peng, R., Ai, L., Zhang, X., Ge, Z., 2015. Efficient polymer solar cells employing a non-conjugated small-molecule electrolyte. Nat. Photon. 9 (8), 520–524.

Qing, J., Zhong, Z.-F., Liu, Y., Li, B.-J., Zhou, X., 2014. MoO₃/Ag/Al/ZnO intermediate layer for inverted tandem polymer solar cells. Chin. Phys. B 23 (3), 038802.

Salim, T., Lee, H.W., Wong, L.H., Oh, J.H., Bao, Z.A., Lam, Y.M., 2016. Semiconducting carbon nanotubes for improved efficiency and thermal stability of polymer-fullerene solar cells. Adv. Funct. Mater. 26 (1), 51–65.

Shim, H.-S., Chang, J.-H., Wu, C.-I., Kim, J.-J., 2014. Effect of different p-dopants in an interconnection unit on the performance of tandem organic solar cells. Org. Electron. 15 (8), 1805–1809.

Shim, J.W., Zhou, Y., Fuentes-Hernandez, C., Dindar, A., Guan, Z., Cheun, H., Kahn, A., Kippelen, B., 2012. Studies of the optimization of recombination layers for inverted tandem polymer solar cells. Sol. Energy Mater. Sol. Cells 107, 51–55.

Sista, S., Hong, Z., Chen, L.-M., Yang, Y., 2011. Tandem polymer photovoltaic cells-current status, challenges and future outlook. Energy Environ. Sci. 4 (5), 1606–1620.

Sun, X.W., Zhao, D.W., Ke, L., Kyaw, A.K.K., Lo, G.Q., Kwong, D.L., 2010. Inverted tandem organic solar cells with a MoO₃/Ag/Al/Ca intermediate layer. Appl. Phys. Lett. 97 (5), 053303.

Sun, Y., Seo, J.H., Takacs, C.J., Seifter, J., Heeger, A.J., 2011. Inverted polymer solar cells integrated with a low-temperature-annealed sol-gel-derived ZnO film as an electron transport layer. Adv. Mater. 23 (14), 1679–1683.

Wang, S.S., Qu, Y.P., Li, S.J., Ye, F., Chen, Z.B., Yang, X.N., 2015. Improved thermal stability of polymer solar cells by incorporating porphyrins. Adv. Funct. Mater. 25 (5), 748–757.

Yang, F., Kim, J.-H., Ge, Z., Kim, Y.-S., 2015. Enhanced thermal stability of inverted polymer solar cells with pentacene. Isr. J. Chem. 55 (9), 1028–1033.

Yang, F., Park, E.-K., Kim, J.-H., Kim, Y.-S., 2016. Improved performance of inverted polymer solar cells using pentacene. Int. J. Energy Res. 40 (5), 677–684.

Yang, J., Zhu, R., Hong, Z., He, Y., Kumar, A., Li, Y., Yang, Y., 2011. A robust inter-connecting layer for achieving high performance tandem polymer solar cells. Adv. Mater. 23 (30), 3465–3470.

Yip, H.-L., Jen, A.K.Y., 2012. Recent advances in solution-processed interfacial materials for efficient and stable polymer solar cells. Energy Environ. Sci. 5 (3), 5994–6011.

You, J., Chen, C.-C., Hong, Z., Yoshimura, K., Ohya, K., Xu, R., Ye, S., Gao, J., Li, G., Yang, Y., 2013a. 10.2% power conversion efficiency polymer tandem solar cells consisting of two identical sub-cells. Adv. Mater. 25 (29), 3973–3978.

You, J., Dou, L., Hong, Z., Li, G., Yang, Y., 2013b. Recent trends in polymer tandem solar cells research. Prog. Polym. Sci. 38 (12), 1909–1928.

You, J., Dou, L., Yoshimura, K., Kato, T., Ohya, K., Moriarty, T., Emery, K., Chen, C.-C., Gao, J., Li, G., Yang, Y., 2013c. A polymer tandem solar cell with 10.6% power conversion efficiency. Nat. Commun. 4, 1446.

Yusoff, A.R.b.M., Lee, S.J., Kim, H.P., Shneider, F.K., da Silva, W.J., Jang, J., 2014. 8.91% power conversion efficiency for polymer tandem solar cells. Adv. Funct. Mater. 24 (15), 2240–2247.

Yusoff, A.R.b.M., Kim, D., Kim, H.P., Shneider, F.K., da Silva, W.J., Jang, J., 2015. A high efficiency solution processed polymer inverted triple-junction solar cell exhibiting a power conversion efficiency of 11.83%. Energy Environ. Sci. 8 (1), 303–316.

Zhou, H., Zhang, Y., Mai, C.-K., Collins, S.D., Bazan, G.C., Nguyen, T.-Q., Heeger, A.J., 2015. Polymer homo-tandem solar cells with best efficiency of 11.3%. Adv. Mater. 27 (10), 1767–1773.

Zhou, Y., Fuentes-Hernandez, C., Shim, J.W., Khan, T.M., Kippelen, B., 2012. High performance polymeric charge recombination layer for organic tandem solar cells. Energy Environ. Sci. 5 (12), 9827–9832.